Electronic Supplementary Information for

Surface N-coordinated Cu catalysts for CO_2 electroreduction to ethylene at industry-level current densities

Huanhuan Tao,[a,b,c] Fang Wang, [a,b,c] Zhengguo Zhang [a,b,c] and Shixiong Min* [a,b,c]

[a]*School of Chemistry and Chemical Engineering, North Minzu University, Yinchuan, 750021, P. R. China.*

[b]*Key Laboratory of Chemical Engineering and Technology, State Ethnic Affairs Commission, North Minzu University, Yinchuan, 750021, P. R. China*

[c]*Ningxia Key Laboratory of Solar Chemical Conversion Technology, North Minzu University, Yinchuan 750021, P. R. China*

*Corresponding authors: sxmin@nun.edu.cn

1. Experimental

1.1 Chemicals and reagents

All chemicals were of analytical grade and used without further purification. Copper nitrate trihydrate ($Cu(NO_3)_2 \cdot 3H_2O$, 99%) and potassium hydroxide (KOH, 90%) were purchased from Shanghai Titan Scientific Co., Ltd. Ammonia solution ($NH_3 \cdot H_2O$, 25-28%) were obtained from Taizhou Shuangshuang Chemical Engineering Co., Ltd. Urea (H_2NCONH_2, 99.0%) was purchased from Tianjin Dengshengxin Chemical Engineering Co., Ltd. The high-purity CO_2 (99.999%) was purchased from Jinghua Industrial Gas Co., Ltd. Ultrapure water (18.2 MΩ cm) was obtained from a water purification system (Hitech ECO-S15).

1.2 Synthesis of catalysts

In details, 0.68 g of $Cu(NO_3)_2 \cdot 3H_2O$ was dissolved in 10 ml of appropriately diluted 28 wt.% ammonia with an aid of ultrasonication for 10 min. After that, 0.3 g of urea was added and ultrasonically mixed for another 10 min. The resulting mixture was then aged in an oil bath at 90 ^oC for 4 h to obtain $Cu(OH)_3NO_3$ precipitates, which were separated by filtration under vacuum, washed with deionized water and ethanol, and dried under in a vacuum oven at 60 ^oC overnight. Finally, the as-obtained $Cu(OH)_3NO_3$ precursor was directly calcined in air at a desirable temperature ranging from 250 to 450 ^oC for 4 h to obtain N-CuO-x precatalysts, where the x represents the calcination temperature. The as-prepared N-CuO-x precatalysts was directly used for the electrocatalytic CO_2 reduction reaction, during which the CuO in N-CuO-x was in situ electrochemically transformed into Cu and the resulting samples were denoted as N-Cu-x. The N-CuO-350 catalyst was further treated by using the ozone cleaning at 750 W for 45 min (Sunlaite, SLT-UVO-02) and the resulting sample was denoted as CuO-350-O.

1.3 Electrochemical measurements

In order to prepare the cathode electrode, the catalyst slurry containing 20 mg catalyst, 1 mL deionized water, 1 mL isopropanol and 25 μL Nafion ionomer solution was mixed and sonicated for 30 min. Then, 1 mL of catalyst slurry was slowly sprayed on GDE at 80 °C to achieve a catalyst loading of ~1.7 mg cm^{-2}. The electrochemical CO_2 reduction experiments were performed in a flow cell (Gaoss union,101017-1.2) with a CS350M electrochemical workstation (Corrtest Instruments, Inc., Wuhan). A Ni foam and a saturated Ag/AgCl were used as the anode and reference electrode, respectively, which were separated by an anion exchange membrane (Fumasep-FAA-3-PK-130). A 1.0 M KOH aqueous solution was utilized as electrolyte and pumped into cathode chamber at a flow rate of 7.5 mL min^{-1}. CO_2 was fed into cathode chamber at a flow rate of 30 mL min^{-1}.[1] Unless otherwise specified, all the applied potentials were reported as revisable hydrogen electrode (RHE) potentials scale using E (*vs*. RHE) =E (*vs.* Ag/AgCl) +1.023 V–IR_s. The solution resistance (R_s) was determined by electrochemical impedance spectroscopy (EIS) measurements, which were performed in a frequency range from 0.01 Hz to 100 kHz at a voltage amplitude of 5 mV. Liner sweep voltammetry (LSV) measurements for the electrodes was carried out in 1 M KOH solution with a scan rate of 10 mV s^{-1}. The gas effluent from the cathodic compartment was delivered directly to the sampling loop of an on-line pre-calibrated gas chromatograph (PANNA GC-A91 plus) equipped with a thermal conductivity detector (TCD) and a flame ionization detector (FID). The Faradaic efficiency (FE) of gaseous products were calculated based on the following Equation (1):

$$FE_i = \frac{Z_i \times G \times V_i \times t \times p_0 \times F \times 10^{-3}}{Q_{total} \times R \times T_0} \times 100\% \quad (1)$$

where Z is the number of electrons transferred; G is volumetric outlet flow rate (27.8

mL min^{-1}); V_i is the volume ratio of gas product i; t is reaction time (min); P_0 and T_0 are atmospheric pressure (101.3 KPa) and reaction temperature (298.15 K); respectively. F is faradaic constant (96485 C mol^{-1}); Q_{total} is integrated charge at each applied potential and R is ideal gas constant (8.314 J·mol^{-1} K^{-1}).

The produced liquid products were quantitatively measured by using the ^{1}H-nuclearmagnetic resonance spectroscopy (^{1}H-NMR) with a Bruker (AVANCE III, 500 MHz). Typically, 2 mL of electrolyte was mixed with D_2O (1 mL) and dimethyl sulfoxide (DMSO, 0.5 mL) for NMR analysis. The FEs of liquid products were calculated by using the following equation (2):

$$FE_{liquid\ products} = \frac{Z_{\text{liquid products}} \times n_{liquid\ products} \times F}{Q_{total}} \times 100\% \qquad (2)$$

where Z is the number of electrons transferred; n is the total amount of product (in moles); respectively. F is faradaic constant (96485 C mol^{-1}); Q_{total} is integrated charge at each applied potential.

The electrochemical surface area (ECSA) of the electrodes was determined by measuring the electric double layer capacitance (C_{dl}). Cyclic voltammetry (CV) tests were performed at different scan rates in a N_2 bubbling 0.1 M $KHCO_3$ electrolyte. The potential window of CV is selected between 0.15-0.25 V, where only double-layer charge and discharge are related. The total charging current at a scan rate of 10-100 mV s^{-1} was determined to be the difference between the anode current and the cathode current at 0.2 V. These capacitive currents are plotted against the scan rate, and the slope of the plot is divided by 2 to obtain the value of C_{dl}.[2]

1.4 Characterizations

X-ray diffraction (XRD) patterns were investigated with a Rigaku smartlab diffractometer with a nickel filtrated Cu Kα radiation in the 2θ range of 5~80° with a

scanning rate of 10° min^{-1}. Scanning electron microscopy (SEM) images were taken with a ZEISS EVO 10 scanning electron microscope. Transmission electron microscopy (TEM) images were taken with a FEI Talos F200x field emission transmission electron microscope. HAADF-STEM observations of the samples were performed on a Titan Cubed Themis G^2 300 STEM. X-ray photoelectron spectroscopy (XPS) measurements of the samples were performed on a ThermoFisher Escalab-250Xi electron spectrometer using an Al Kα X-ray source. Binding energies were referenced to the C 1s peak (set at 284.8 eV) of the sp^2 hybridized (C=C) carbon from the sample.

2. Additional data

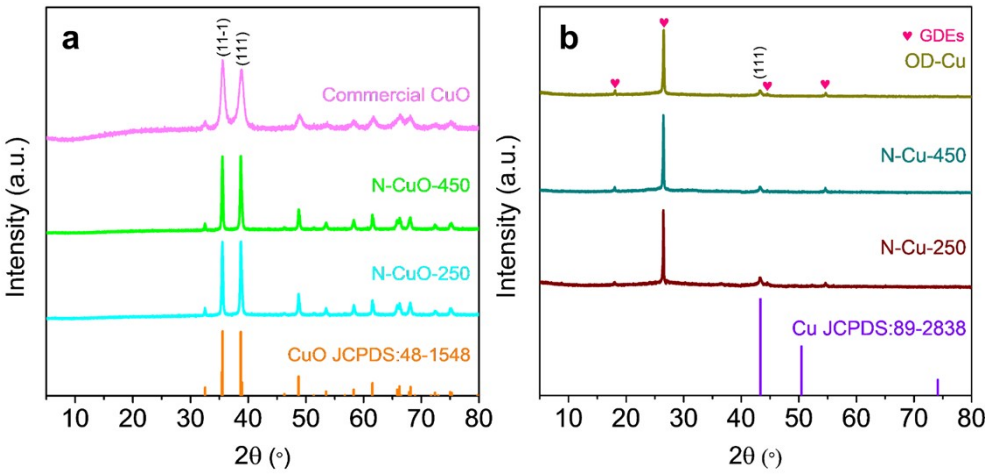

Fig. S1 XRD patterns of (a) N-CuO-250, N-CuO-450, and commercial CuO and (b) N-Cu-250, N-Cu-450, and OD-Cu.

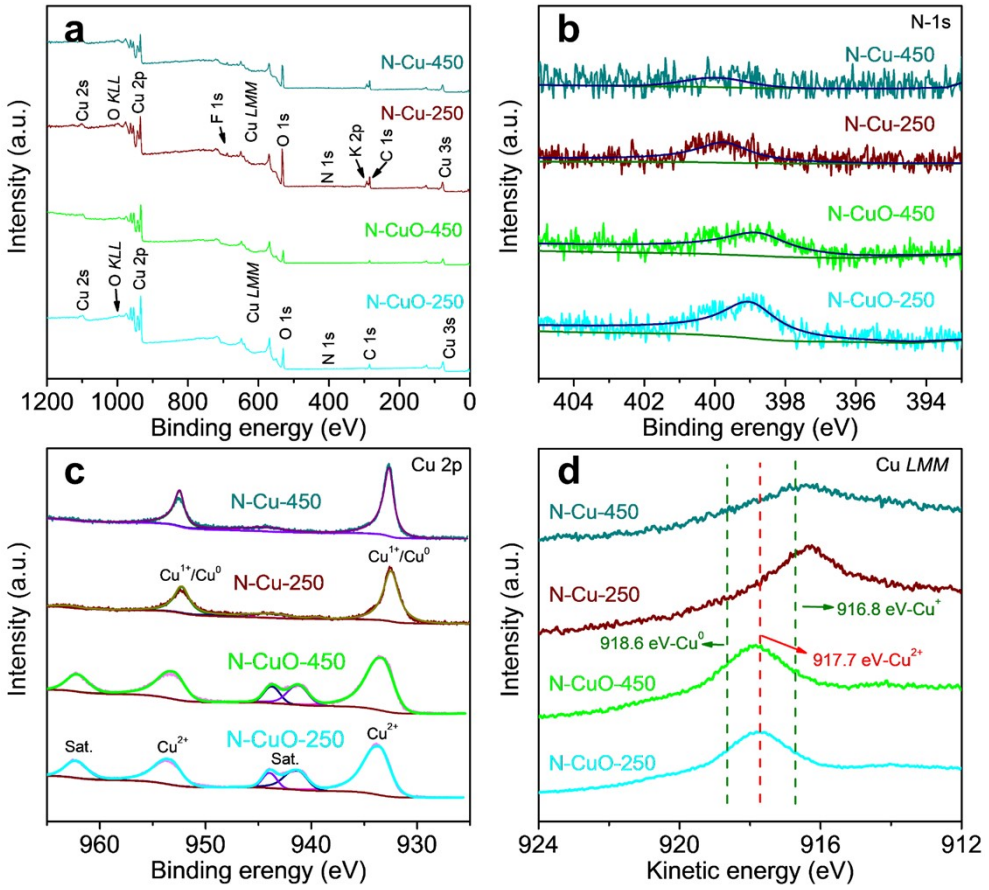

Fig. S2 (a) Survey, (b) N 1s, (c) Cu 2p, and (d) Cu *LMM* Auger XPS spectra of N-Cu-250, N-Cu-450, N-CuO-250, and N-CuO-450.

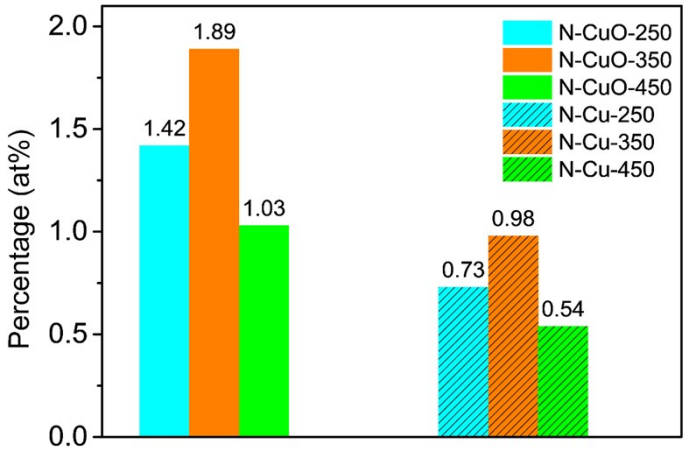

Fig. S3 The surface N content of N-CuO-x and N-Cu-x.

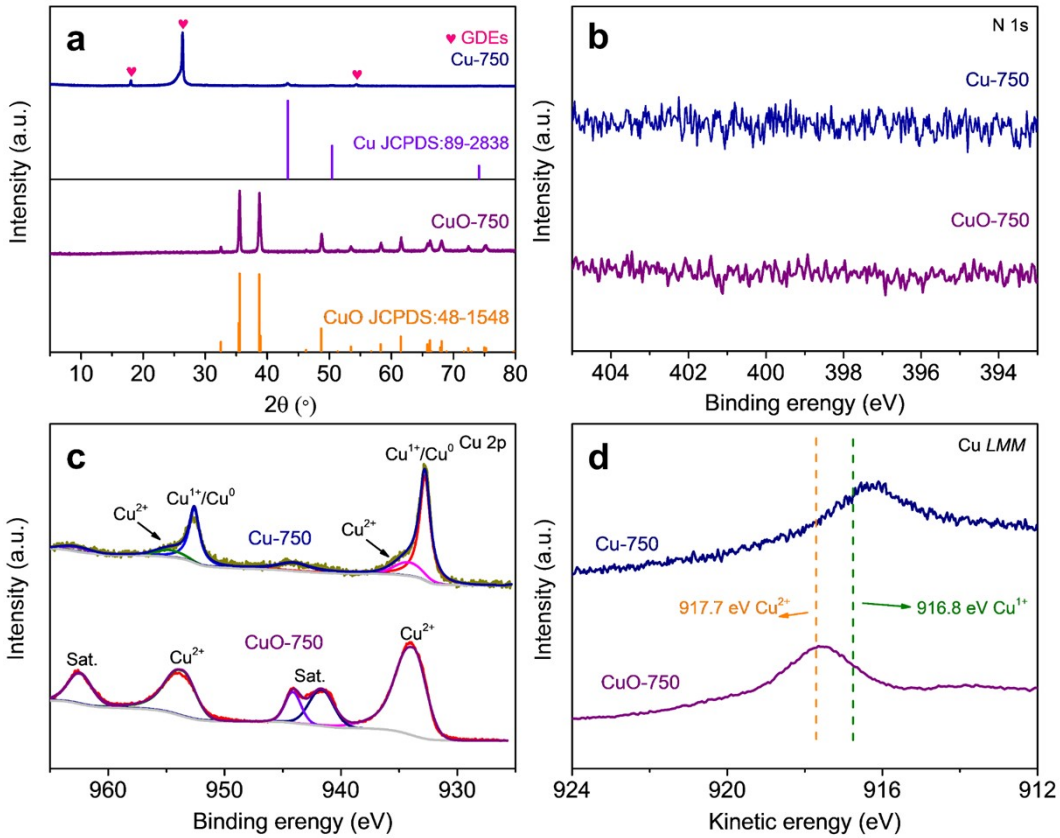

Fig. S4 (a)XRD patterns of CuO-750 and Cu-750. (b) N 1s, (c) Cu 2p, and (d) Cu *LMM* Auger XPS spectra of CuO-750 and Cu-750.

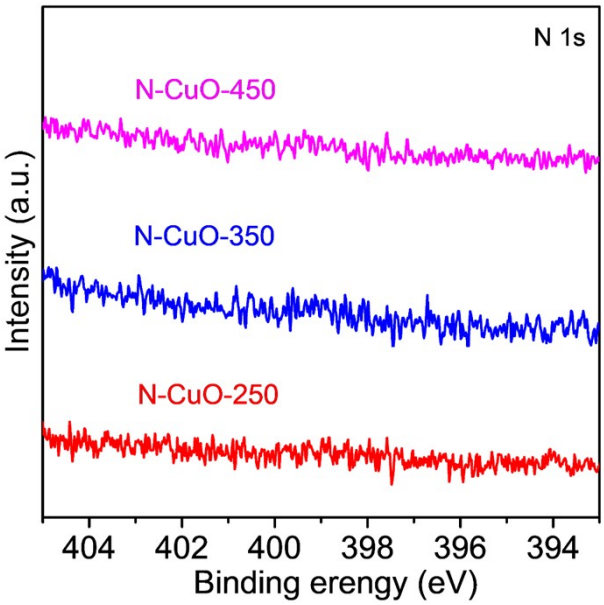

Fig. S5 N 1s XPS spectra of N-CuO-250, N-CuO-350, and N-CuO-450 after Ar^+ etching for 70 s.

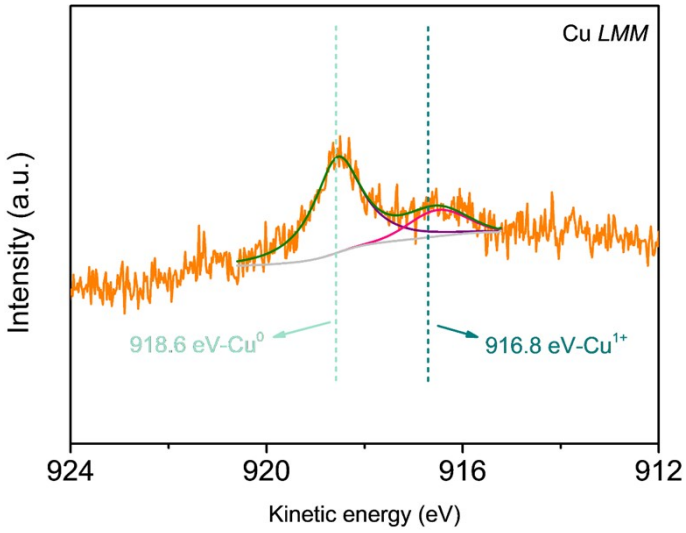

Fig. S6 Cu *LMM* Auger XPS spectrum of N-Cu-350 prepared in glovebox under the protection of N_2 atmosphere. After the CO_2RR, the flow cell was transferred into the glovebox and the electrode was taken out under the protection of N_2 atmosphere. After dying with N_2 flow in glovebox, the electrode was directly mounted onto the sample stage of a transfer chamber for XPS analysis.

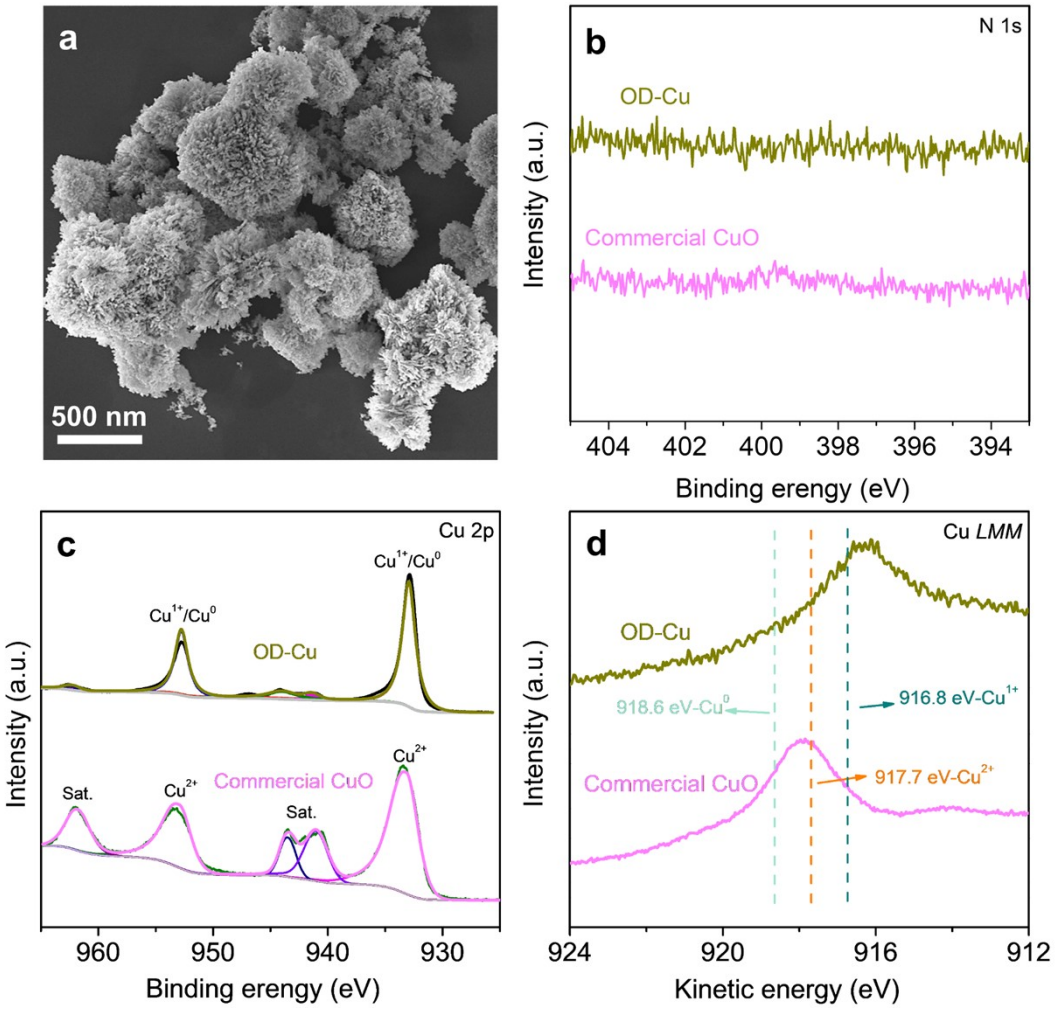

Fig. S7 (a) SEM image of commercial CuO. (b) N 1s, (c) Cu 2p, and (d) Cu *LMM* Auger XPS spectra of commercial CuO and OD-Cu.

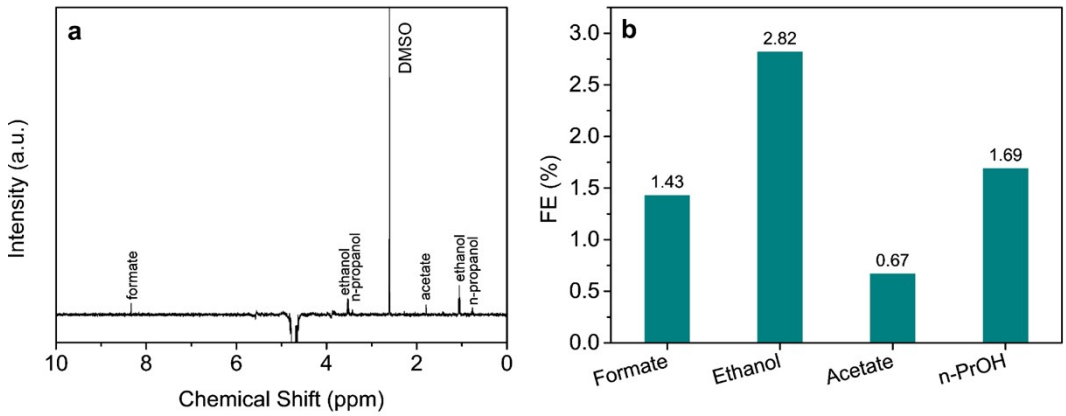

Fig. S8 A representative ^{1}H-NMR spectrum of catholyte for the CO_2RR over N-Cu-350 at -1.09 V vs. RHE and (b) the corresponding FEs of liquid products.

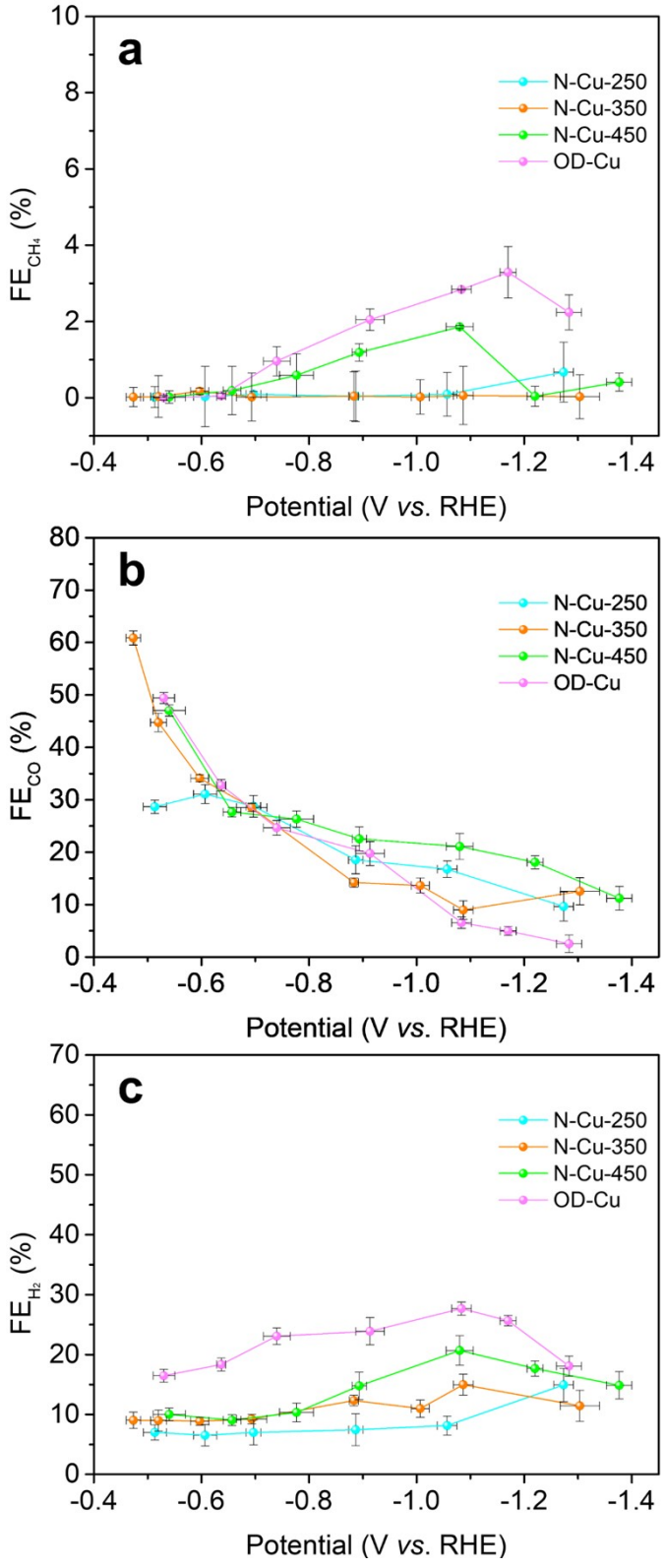

Fig. S9 FEs of CH_4, (b) CO, and (c) H_2 over N-Cu-250, N-Cu-350, N-Cu-450 and OD-Cu as a function of applied potential.

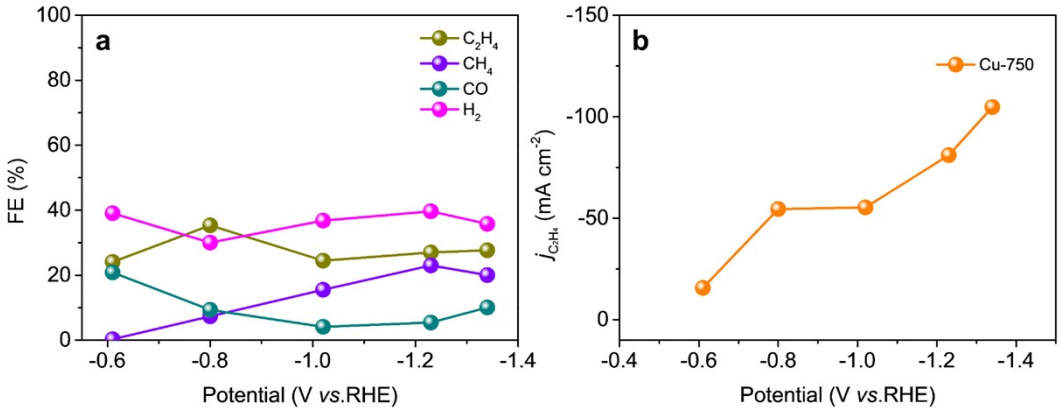

Fig. S10 (a) FEs of CO_2 reduction products and (b) partial current density of C_2H_4 over Cu-750 as a function of applied potentials.

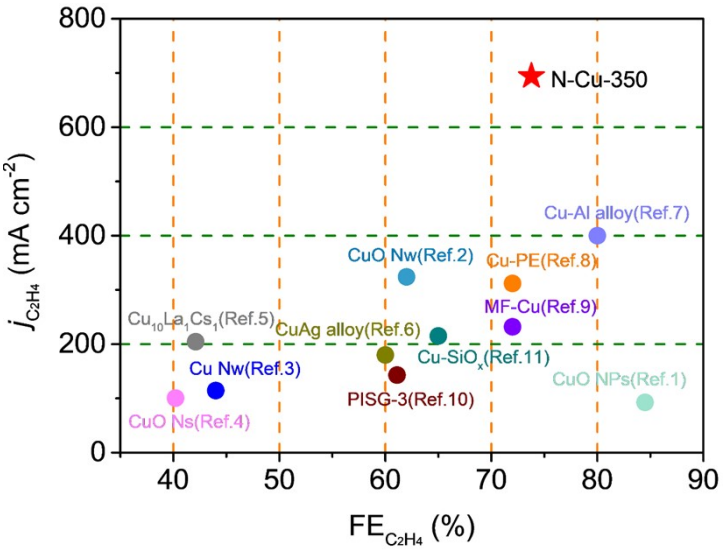

Fig.S11 C_2H_4 FE and partial current density in the CO_2RR reported in the literatures.

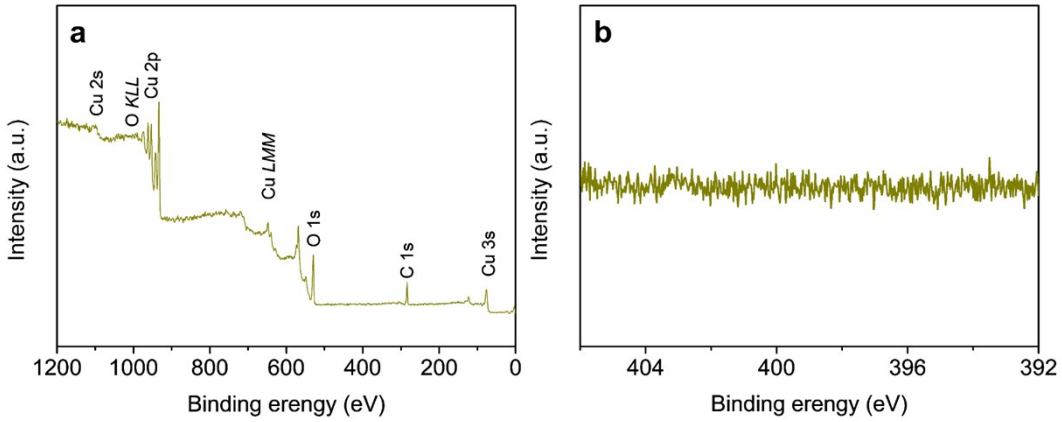

Fig. S12 (a) XPS survey and (b) N 1s XPS spectra of CuO-350-O.

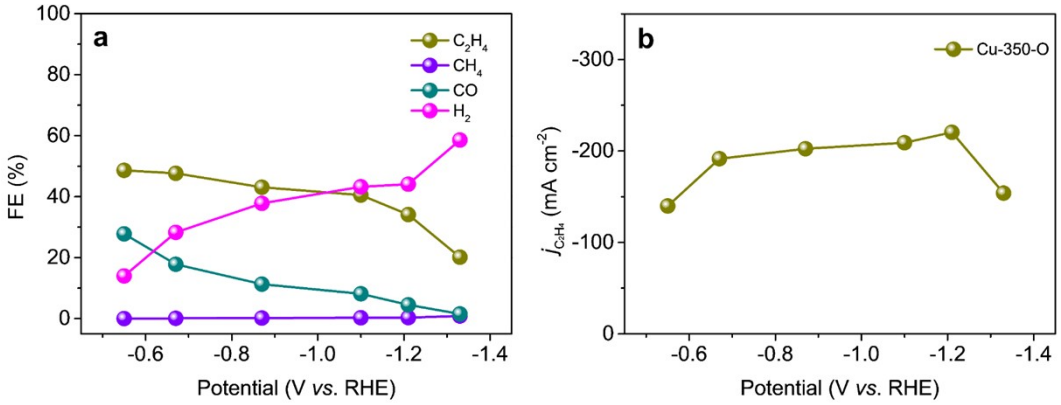

Fig. S13 (a) FEs of CO_2 reduction products and (b) partial current density of C_2H_4 over Cu-350-O as a function of applied potentials.

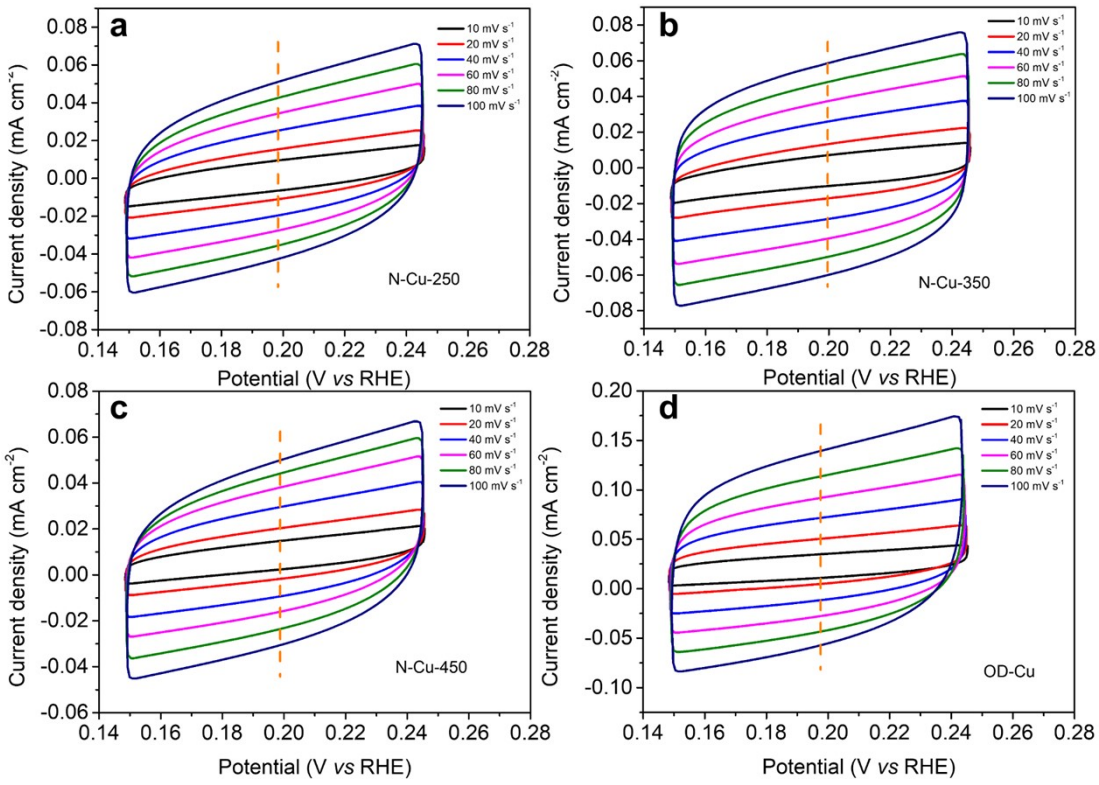

Fig. S14 CV curves at different scan rates in the non-Faradaic capacitance range of (a) N-Cu-250, (b) N-Cu-350 (c) N-Cu-450, and (d) OD-Cu.

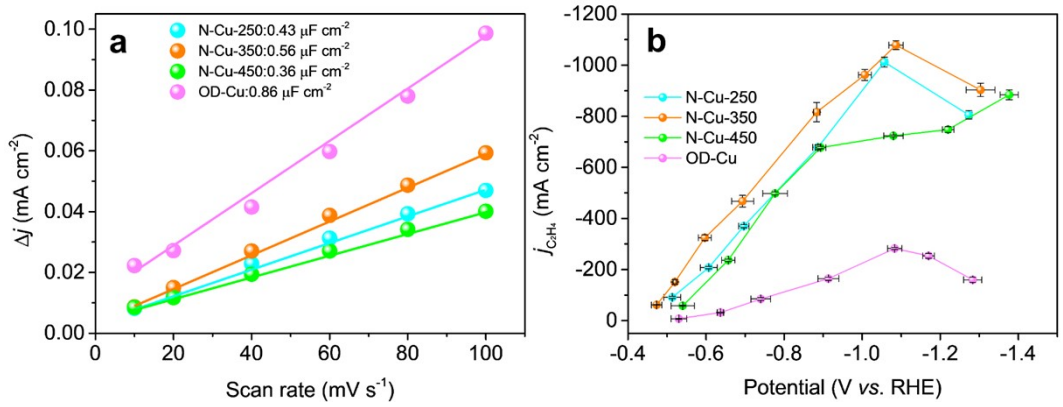

Fig. S15 (a) Current density plotted against scan rate of N-Cu-250, N-Cu-350, N-Cu-450, and OD-Cu. (b) ECSA-normalized partial current densities of C_2H_4 production on N-Cu-250, N-Cu-350, N-Cu-450, and OD-Cu.

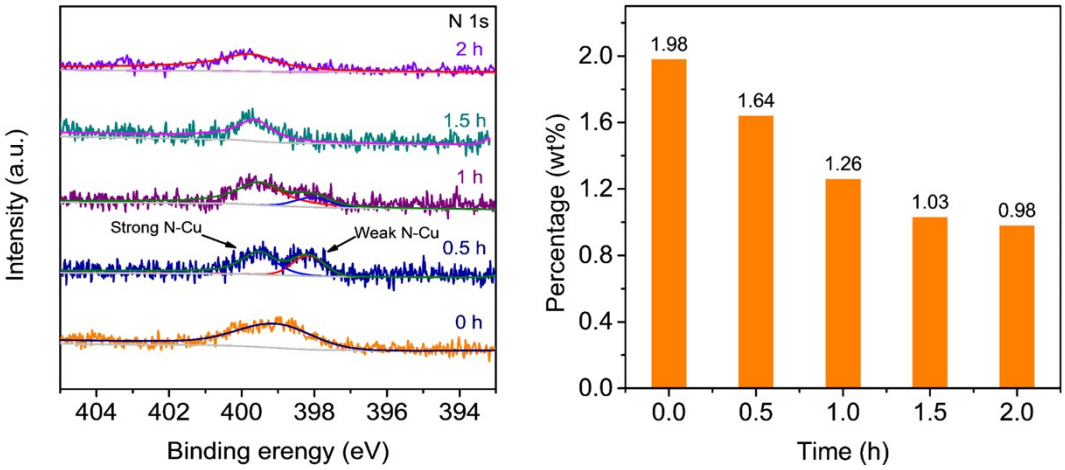

Fig. S16 (a) N 1s XPS spectra and (b) the corresponding surface N content of N-Cu-350 electrode at different times of the CO_2RR.

References

1 H. Chang, H. Pan, F. Wang, Z. Zhang, Y. Kang and S. Min, *Nanoscale*, 2022, **14**, 10003-10008.

2 W. Deng, S. Min, F. Wang, Z. Zhang and C. Kong, *Dalton Trans.*, 2020, **49**, 5434-5439.

3 W. Liu, P. Zhai, A. Li, B. Wei, K. Si, Y. Wei, X. Wang, G. Zhu, Q. Chen, X. Gu, R. Zhang, W. Zhou and Y. Gong, *Nat. Commun.*, 2022, **13**, 1877.

4 J. Zhang, Z. Li, S. Xia, T. Zhang, Y. Wang, Y. Wu and J. Wu, *Chem. Commun.*, 2021, **57**, 8276-8279.

5 H. S. Jeon, J. Timoshenko, C. Rettenmaier, A. Herzog, A. Yoon, S. W. Chee, S. Oener, U. Hejral, F. T. Haase and B. Roldan Cuenya, *J. Am. Chem. Soc.*, 2021, **143**, 7578-7587.

6 M. Wang, L. Wan, J. Cheng and J. Luo, *J. Mater. Chem. A*, 2022, **10**, 14070-14077.

7 1S. Jia, Q. Zhu, H. Wu, S. Han, M. Chu, J. Zhai, X. Xing, W. Xia, M. He and B. Han, *Chem. Sci.*, 2022, **13**, 7509-7515.

8 T. T. H. Hoang, S. Verma, S. Ma, T. T. Fister, J. Timoshenko, A. I. Frenkel, P. J. A. Kenis and A. A. Gewirth, *J. Am. Chem. Soc.*, 2018, **140**, 5791-5797.

9 M. Zhong, K. Tran, Y. Min, C. Wang, Z. Wang, C. T. Dinh, P. De Luna, Z. Yu, A. S. Rasouli, P. Brodersen, S. Sun, O. Voznyy, C. S. Tan, M. Askerka, F. Che, M. Liu, A. Seifitokaldani, Y. Pang, S. C. Lo, A. Ip, Z. Ulissi and E. H. Sargent, *Nature*, 2020, **581**, 178-183.

10 X. Chen, J. Chen, N. M. Alghoraibi, D. A. Henckel, R. Zhang, U. O. Nwabara, K. E. Madsen, P. J. A. Kenis, S. C. Zimmerman and A. A. Gewirth, *Nat. Catal.*, 2020, **4**, 20-27.

11 F. Li, A. Thevenon, A. Rosas-Hernandez, Z. Wang, Y. Li, C. M. Gabardo, A. Ozden, C. T. Dinh, J. Li, Y. Wang, J. P. Edwards, Y. Xu, C. McCallum, L. Tao, Z. Q. Liang, M. Luo, X. Wang, H. Li, C. P. O'Brien, C. S. Tan, D. H. Nam, R. Quintero-Bermudez, T. T. Zhuang, Y. C. Li, Z. Han, R. D. Britt, D. Sinton, T. Agapie, J. C. Peters and E. H. Sargent, *Nature*, 2020, **577**, 509-513.

12 R.-X. Yang, Y.-R. Wang, G.-K. Gao, L. Chen, Y. Chen, S.-L. Li and Y.-Q. Lan, *Small Struct.*, 2021, **2**.2100012

13 J. Li, A. Ozden, M. Wan, Y. Hu, F. Li, Y. Wang, R. R. Zamani, D. Ren, Z. Wang, Y. Xu, D. H. Nam, J. Wicks, B. Chen, X. Wang, M. Luo, M. Graetzel, F. Che, E. H. Sargent and D. Sinton, *Nat. Commun.*, 2021, **12**, 2808.